Thin Solid Films 518 (2010) 6997–7001

Contents lists available at ScienceDirect

Thin Solid Films

journal homepage: www.elsevier.com/locate/tsf

Temperature dependence of resistance and thermopower of thin indium tin oxide films

Bo-Tsung Lin [a], Yi-Fu Chen [a], Juhn-Jong Lin [a,b], Chih-Yuan Wu [c,*]

[a] Institute of Physics, National Chiao Tung University, Hsinchu 30010, Taiwan
[b] Department of Electrophysics, National Chiao Tung University, Hsinchu 30010, Taiwan
[c] Department of Physics, Fu Jen Catholic University, Hsinchuang 24205, Taiwan

ARTICLE INFO

Article history:
Received 16 May 2009
Received in revised form 31 May 2010
Accepted 5 June 2010
Available online 12 June 2010

Keywords:
Indium tin oxide
Electronic conduction
Electron–electron interaction
Weak-localization effect

ABSTRACT

We have measured the resistance and thermopower of a series of RF sputtered and annealed indium tin oxide (ITO) thin films from 300 K down to liquid-helium temperatures. Thermal annealing was performed to modulate the levels of disorder (i.e., resistivity) of the samples. The measured resistances are well described by the Bloch–Grüneisen law between 150 and 300 K, suggesting that our thin films are metallic. At lower temperatures, a resistance rise with decreasing temperature was observed, which can be quantitatively ascribed to the two-dimensional electron–electron interaction and weak-localization effects. The thermopowers in all samples are negative and reveal fairly linear temperature dependence over the whole measurement temperature range, strongly indicating free-electron like conduction characteristics in ITO thin films. As a result, the carrier concentration in each film can be reliably determined. This work demonstrates that ITO films as thin as 15 nm thick can already possess high metallic conductivity.

© 2010 Elsevier B.V. All rights reserved.

1. Introduction

Indium tin oxide (known as ITO) films exhibiting high visible transparency and low electrical resistivity have been extensively used in optoelectronic applications. For example, ITO films are used as transparent electrodes in flat panel displays, resistive touch panels, and solar cells [1–4]. They are also used as the anode contacts in organic light-emitting diodes and flexible displays. In recent years, in view of the technological applications, many of the studies of ITO have focused on the following three directions. First, concerning growth methods, there are several deposition techniques commonly utilized to grow ITO, including the thermo growth method, the pulsed laser deposition method, and the reactive electron-beam deposition method. The objective is to investigate how the various growth techniques might cause different electrical and optical properties. Second, regarding the optical phenomena, the optical constant, reflectance, transmittance and absorption coefficient spectrum have been widely investigated. The third direction is connected with the ITO as a transparent electrode material. The contact resistance between an ITO electrode and a display device undoubtedly plays an important role in the performance of any optoelectronic products. Plasma treatments have thus been suggested to improve device performance. All these works have established that ITO is a degenerate wide-gap semiconductor with a band gap of 3.5–4.5 eV, rendering a high transmittance in the visible region and a high reflectance in the infrared region. As for electrical properties, the resistivities of properly deposited (and thermally treated) ITO thick films can be reduced to be as low as ~200 μΩ cm, while the carrier concentrations can be raised to be as high as $\sim 10^{20}$–10^{21} electrons/cm^3 at room temperature [1,3–5].

In contrast to the above-mentioned works aiming on the technological sides, studies of the electronic conduction properties in ITO over a wide range of temperature from 300 K down to liquid-helium temperatures are much limited. Very recently, Liu et al. [6] have fabricated amorphous as well as polycrystalline ITO thick films (210–370 nm thickness) by adjusting the growth conditions. They observed a metallic conduction in polycrystalline samples, while a semiconducting behavior in amorphous samples. For their metallic samples between 100 and 300 K, they compared the measured resistance data with the Bloch–Grüneisen (B–G) law and obtained a Debye temperature of 1040 K and an electron–phonon coupling constant $\beta = 0.35$–0.54 μΩ cm/K [see Eq. (1) below for the definition of β]. At lower temperatures, a correction to the residual resistivity due to the three-dimensional electron–electron interaction effects was identified. Li and Lin [7] measured the resistances and thermopowers (Seebeck coefficients) for 125- and 240-nm thick ITO films. Their results pointed out that the temperature behavior of resistance is metallic, with the weak-localization and electron–electron interaction effects being important at liquid-helium temperatures, while the thermopowers were negative and essentially linear in temperature between 2 and 300 K. Ederth et al. [3,4] have investigated thick ITO nanoparticle films. They found that the resistance increased with reducing temperature for all temperatures below 300 K. They

* Corresponding author. Tel.: +886 2 29052533; fax: +886 2 29021308.
E-mail address: 016287@mail.fju.edu.tw (C.-Y. Wu).

0040-6090/$ – see front matter © 2010 Elsevier B.V. All rights reserved.
doi:10.1016/j.tsf.2010.06.010

interpreted their results in terms of the thermal fluctuation-induced tunneling conduction [8,9] between ITO clusters of individually connected nanoparticles. Moreover, after annealing at 800 K, their samples displayed a metallic-like behavior between 150 and 300 K. Kikuchi et al. [10] have measured the Hall effect and determined the carrier concentrations, *n*, in a series of ITO films. They found that *n* is independent of temperature between 6 and 300 K. On the theoretical side, Mryasov and Freeman [11], and Odaka et al. [12] have calculated the electronic band structure of Sn-doped In_2O_3. The two theoretical groups reached the similar conclusion that doping of a few at.% of Sn into In_2O_3 could give rise to free-electron-like carriers, and thus resulting in metallic behaviors, in ITO.

In this work, our objective is to experimentally investigate the electronic transport properties in metallic ITO *thin* films containing different amounts of disorder. Our films are 15-nm thick, while all the aforementioned studies of ITO have focused on much thicker films. We have determined the relevant physical quantities, such as the Debye temperature, electron–phonon coupling constant, Fermi energy, and carrier concentration, from resistance together with thermopower measurements. In addition, we have observed two-dimensional weak-localization and electron–electron interaction effects from resistance measurements at low temperatures. Our results indicate that RF sputtered thin ITO films can already demonstrate high metallic conductivity.

2. Experimental method

Our ITO film was deposited by the RF sputtering method on a 20×50 cm^2 rectangular glass substrate, and was supplied by the RITEK Corporation. The ITO film was 15-nm thick and the composition was $In_{2-y}Sn_yO_{3-\delta}$, with $y = 0.195$, as specified by the supplier. In this work, three pieces of as-sputtered samples were cut from different locations of the large glass substrate. In addition, three more pieces of samples were cut and thermally annealed in a flowing Ar gas. The samples were heated to 300 °C (500 °C, 550 °C) at a rate of 5 °C/min, and then kept at the target temperature for 1 h. After annealing, the samples were cooled down to room temperature at a rate of 5 °C/min in the flowing Ar gas. Thermal annealing led to a reduced carrier concentration (as determined from thermopower measurement, see below), and thus an increased resistivity. The relevant parameters of our samples studied in this work are listed in Table 1.

Four-probe resistance measurements were carried out using a Linear Research LR-700 resistance bridge. The samples were mounted on the sample holder of either a standard ^{4}He or a ^{3}He cryostat. The temperature was monitored with a calibrated RuO_2 thermometer. Applying a measuring current of 0.3 μA and employing a high-precision circuitry with a sensitivity of ≤10 nV [13], we were able to achieve a signal resolution in the relative resistance change of $\Delta R/R \approx 1.5 \times 10^{-5}$.

The thermopower *S* was measured by a steady dc technique [7]. A temperature gradient across the sample (typically, ~1-cm long and 3-mm wide) was generated by a 1-kΩ surface mount resistor anchored at the hot end. The temperatures in the cold and hot ends were measured with a Chromel-constantan thermocouple thermometer. Thin Pb wires (0.25 mm diameter) were used for the voltage leads, because the thermopower of Pb in the normal state is well tabulated in the literature [14].

Table 1
Values of relevant parameters for ITO thin films. T_a is the annealing temperature. [a]For some unknown reasons, the temperature behavior of resistance for the A1 film could not be satisfactorily described by Eq. (1).

Sample	ρ(300 K) (μΩ cm)	ρ_0 (μΩ cm)	T_a (°C)	θ_D (K)	β (μΩ cm/K)	E_F (eV)	n (10^{20}/cm^3)
n1	853	823	nil	1085	0.75	0.56	4.8
n2	693	668	nil	1026	0.60	0.62	5.6
n3	767	733	nil	1071	0.71	0.52	4.3
A1[a]	966	1003	300	–	–	0.48	3.8
A2	1105	1069	500	1018	0.80	–	–
A3	1169	1125	550	1020	1.02	0.37	2.6

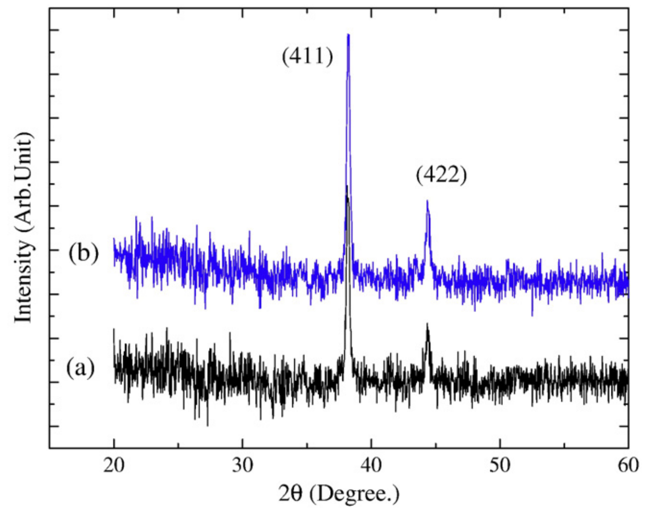

Fig. 1. XRD patterns for the as-deposited n2 film (curve a) and the thermal-annealed A3 film (curve b).

3. Results and discussion

The atomic structure of our films was determined by the x-ray diffraction (XRD) measurement, and the film microstructure and morphology was examined by the scanning electron microscopy (SEM). Fig. 1 shows the XRD patterns of a representative as-deposited (curve a) and a representative thermal-annealed (curve b) ITO films, respectively. The two films reveal similar diffraction patterns, where the maximum intensity peak corresponds to the (411) preferential orientation while the minor peak corresponds to the (422) peak, as indicated. This observation suggests that our films are polycrystalline, rather than amorphous. Fig. 2(a) and (b) shows the microstructures of the representative n2 and A3 films, respectively. Close inspection indicates that our films are composed of relatively small grains, while there was absence of notable pores. The average grain size is 17–25 nm. Such a small mean grain size (and thus, there should be strong grain boundary scattering of conduction electrons) leads to the relatively high resistivity of ρ(300 K) ~ 1000 μΩ cm found in our thin films. For comparison, the room-temperature resistivity is often of ~150 μΩ cm in high-quality thick (≥100 nm) ITO films where the grain sizes are typically of ~50 nm or larger [15,16]. Moreover, we notice that thermal annealing of our thin films resulted in a slightly increased grain size, accompanied with a reduced carrier concentration (see Table 1). As a consequence, the resistivity of the film increased.

3.1. Metallic conduction in resistance and thermopower

Fig. 3(a) shows the normalized resistivity $\rho(T)/\rho(300\,K)$ as a function of temperature for three representative ITO thin films between 100 and 300 K. The symbols are the experimental data. Note that, for clarity, the data for the A3 (n3) film has been vertically shifted up (down) by an amount of 0.01 (−0.01).

The temperature behavior of resistivity of a normal metal is given by the Bloch–Grüneisen (B–G) law [17]

$$\rho = \rho_0 + \beta T \left(\frac{T}{\theta_D}\right)^4 \int_0^{\theta_D/T} \frac{x^5 dx}{(e^x - 1)(1 - e^{x})}, \quad (1)$$

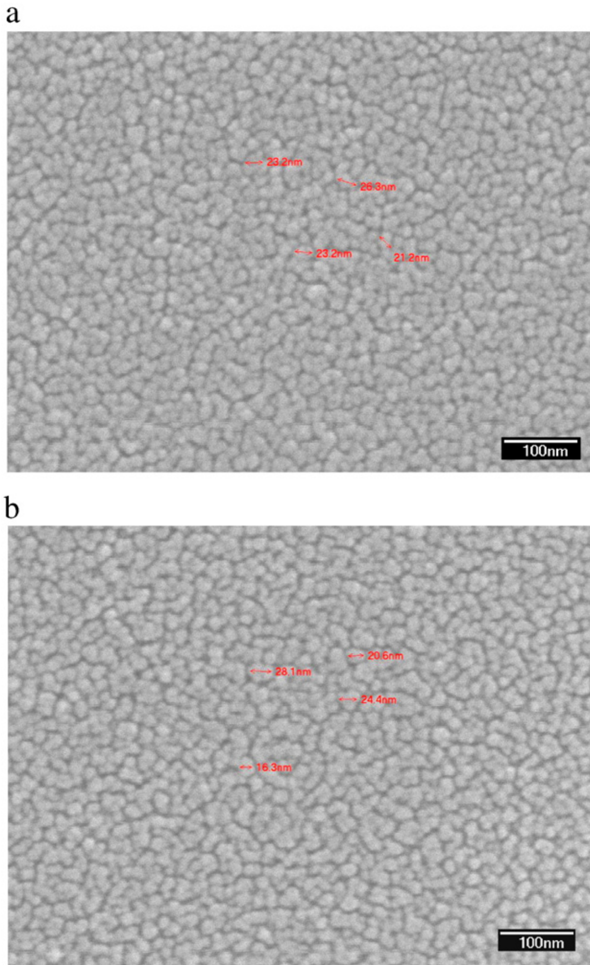

Fig. 2. SEM micrographs of (a) the as-deposited n2 film, and (b) the thermal-annealed A3 film. Notice that the grain size is approximately 17–25 nm.

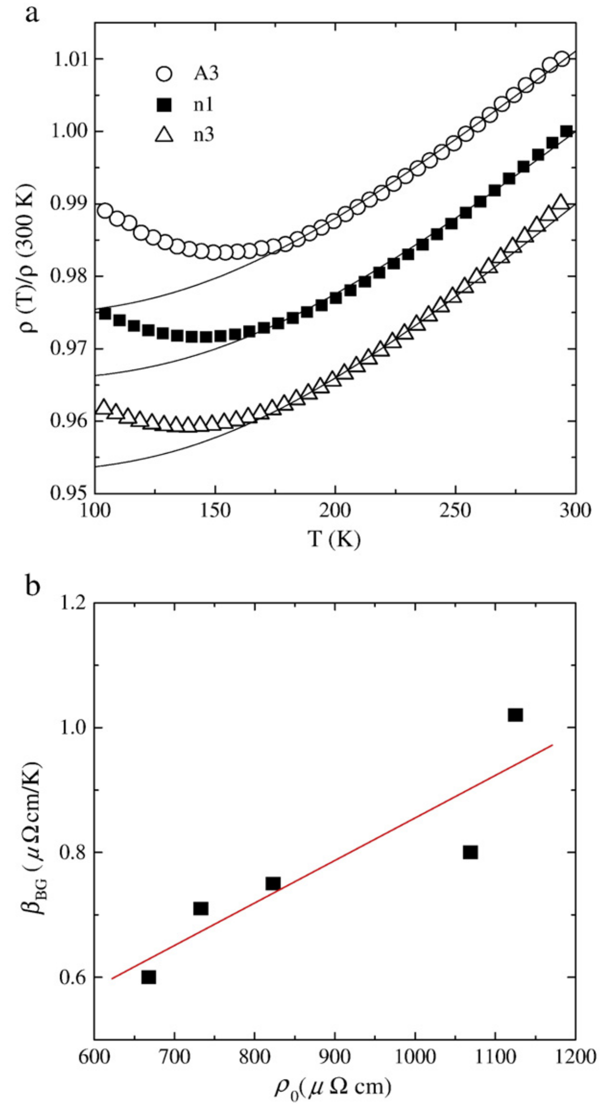

Fig. 3. (a) Normalized resistivity, $\rho(T)/\rho(300\ K)$, as a function of temperature for three representative ITO thin films, as indicated. The solid curves are least-squares fits to the predictions of Eq. (1). Notice that, for clarity, the data for the A3 (n3) film has been vertically shifted up (down) by an amount of 0.01 (−0.01). (b) Variation of the electron–phonon coupling constant β with residual resistivity ρ_0. The straight solid line is a guide to the eye.

where ρ_0 is a residual resistivity, β is an electron–phonon coupling constant, θ_D is the Debye temperature, and $x = \hbar\omega_q/k_BT$ (where ω_q is the phonon frequency). In Fig. 3(a), the solid curves are the least-squares-fits of Eq. (1) to the samples for the temperature range of ~150 to 300 K. It is seen that the B–G law can well describe our results in this temperature range. In other words, the electrical conduction behavior in our ITO thin films is metallic. The increase in resistance with increasing temperature is due to electron–phonon scattering. Our extracted values of β and θ_D are listed in Table 1. These values are in good agreement with the corresponding values recently reported by Li and Lin [7], and Liu et al. [6] for ITO thick films, and by Chiu et al. [18] for ITO single-crystalline nanowires.

Within the framework of the B–G model, the electron–phonon coupling constant β in Eq. (1) should be independent of the amount of disorder in the sample. However, we found that our experimental β value increases essentially linearly with increasing residual resistivity ρ_0 of the film, see Fig. 3(b). Such a linear disorder behavior of β has recently been found in AuPd thick films [19] and zinc-doped indium oxide films [20]. In the latter case, the authors noticed that the measured ρ_0 dependence of β came from the disorder dependence of carrier concentration n but not from other electronic properties. More precisely, they found in Zn-doped indium oxide films $\rho_0 \propto 1/n$, and hence $n\beta$ is constant. In the case of our ITO thin films, the product $n\beta \approx 3.1 \pm 0.5\ \mu\Omega/\mathrm{K\ cm}^2$ also remains roughly constant (see below for our experimental determination of n). However, it should be noted that such an explanation cannot be carried over to the case of AuPd thick films. In AuPd thick films, Yeh et al. [19] have found that their β value varied by a factor of ~3 from 0.1 to 0.3 μΩ cm/K as ρ_0 changed from 40 to 280 μΩ cm. Such a huge variation by three times certainly cannot be accounted for by a corresponding change in n, since AuPd is a metal alloy where n is essentially constant and insensitive to disorder. It is conjectured that this anomalous disorder behavior of β might result from an electron–phonon-impurity interference effect [21] which is not taken into consideration in Eq. (1). This issue deserves further theoretical investigation.

In a typical metal, the thermopower (Seebeck coefficient) comprises two contributions: the diffusion thermopower and the phonon-drag thermopower. The diffusion thermopower is given by [14]

$$S \approx -\frac{\pi^2 k_B^2 T}{3|e|E_F}, \qquad (2)$$

where k_B is Boltzmann's constant, e is the electronic charge, and E_F is the Fermi energy. In the presence of a high level of disorder, the phonon-drag term is expected to be suppressed. Fig. 4 shows our measured thermopowers as a function of temperature for five ITO thin films between 10 and 300 K. The symbols are the experimental data and the straight solid lines are least-squares-fits to Eq. (2). It is clearly

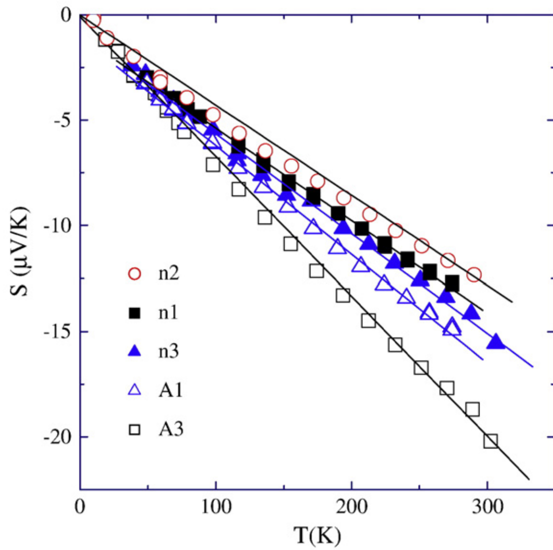

Fig. 4. Thermopower as a function of temperature for five ITO thin films, as indicated. The straight solid lines are least-squares fits to Eq. (2).

seen that the thermopowers are negative and basically linear in temperature for the whole measurement temperature range. The negative sign indicates electron, rather than hole, conduction, while the linearity confirms that the phonon-drag contribution is negligibly small. Indeed, the robust linearity strongly suggests that the conduction process in ITO films as thin as 15 nm thick is already free-electron-like. This observation is in line with the metallic behavior of resistance found in Fig. 3(a). A linear thermopower over the whole relevant range of temperature shall render the extraction of carrier concentration n in the sample very accurate.

The difference in the slopes of the straight solid lines in Fig. 4 indicates a change in the Fermi energy E_F (or, equivalently, carrier concentration n) in our ITO thin films due to thermal annealing. Our experimental values of E_F are listed in Table 1. Table 1 also lists the values of n which were deduced through the relation $E_F = (\hbar^2/2m^*)(3\pi^2 n)^{2/3}$, by using an effective mass $m^* = 0.4\,m$ [7], where m is the free electron mass. Our values of n (≈ 2.6–5.6×10^{20} electrons/cm^3) are in line with those reported in the literature for ITO materials with compatible resistivities [2–4,6,9,19,22]. It is worth noting that thermal annealing is a very effective way for changing the carrier concentration in ITO. This method has been widely applied by many groups in the hope to increase n, and hence to reduce ρ, in these materials [23,24]. In a number of previous studies [2,24–27], the Hall effect measurements were carried out to determine n. The thermal annealing was usually carried out in temperatures between 200 °C and 550 °C. An increase in n was found when the ITO films were annealed in a vacuum [27] (n increased by an amount of ~100%), in nitrogen [2,25] (n increased by an amount of ~200%), and in air [2] (n increased by an amount of ~10%). On contrary, other studies have reported a decrease in n when the samples were annealed in oxygen [9] (n decreased by an amount of ~20%), and in air [26,27] (n decreased by an amount of ~30%). As for the present study, we found a decrease in n by an amount of ~35%. These experimental results are obviously inconsistent with each other. This issue of the effect of thermal annealing on changing n warrants further systematic studies, especially considering that high-quality electrical conduction is of crucial importance for the applications of ITO films.

3.2. Quantum-interference corrections to low-temperature resistance

Both the electron–electron interaction and weak-localization effects result in notable contributions to the temperature dependence of resistance in low-dimensional systems at low temperatures. In two dimensions, the sum of the corrections to the sheet resistance, $R_\square$, due to these two effects is given by [28]

$$\frac{\Delta R_\square(T)}{R_\square^2(T_0)} = -\frac{e^2}{2\pi^2\hbar}\left[\alpha p + \left(1-\frac{3}{4}F\right)\right]\ln\left(\frac{T}{T_0}\right), \tag{3}$$

where $R_\square$ is the sheet resistance, α is a constant, p is the exponent of temperature for the responsible electron dephasing time τ_φ ($\propto T^{-p}$), F is an electron screening factor, and T_0 is an arbitrary reference temperature (taken to be 20 K in the present work). In ITO, the spin-orbit scattering is negligibly small and $\alpha = 1$. In two dimensions, $p = 1$ for not too low temperatures where the Nyquist electron–electron scattering is the dominant dephasing process, while $p < 1$ at very low temperatures if there is a saturation in τ_φ [29–31]. In this work, we have measured the resistance in each film down to 0.3 K in both zero magnetic field and in a perpendicular magnetic field of 4 T. Such complementary measurements allow us to quantitatively separate the weak-localization and electron–electron interaction effects in ITO thin films.

Fig. 5 shows the normalized sheet resistance, $\Delta R_\square(T)/R_\square^2(20\text{ K}) = [R_\square(T) - R_\square(20\text{ K})]/R_\square^2(20\text{ K})$, as a function of the logarithm of the normalized temperature T/T_0 for the n1 thin film. (All the other films behave very similarly, and thus are not shown.) The sheet resistance $R_\square(T_0) = \rho(T_0)/t = 574\ \Omega$, where $t = 15$ nm is the film thickness. The symbols are the experimental data and the straight lines are the predictions of Eq. (3). In the presence of a perpendicular magnetic field of 4 T, the weak-localization effect is suppressed, and thus the logarithmic increase in the normalized sheet resistance (circles) is totally due to the electron–electron interaction effects. Our least-squares fits in this case give the value $1 - 3F/4 = 0.91$, suggesting a value of $F = 0.12$. In zero magnetic field, the temperature behavior of sheet resistance is slightly more complicated. The extra resistance rise (i.e., the difference between the square and the circle at a given temperature) can be ascribed to the contribution from the weak-localization effect.

A least-squares-fit to the straight solid line through the squares indicates a slope of $\alpha p + 1 - 3F/4 = 1.91$. Therefore, $\alpha p = 1.0$ in this particular film, suggesting that $p = 1$. We notice that, below about 4 K, the rise in sheet resistance due to the weak-localization effect gradually slows down with reducing temperature. This behavior can be

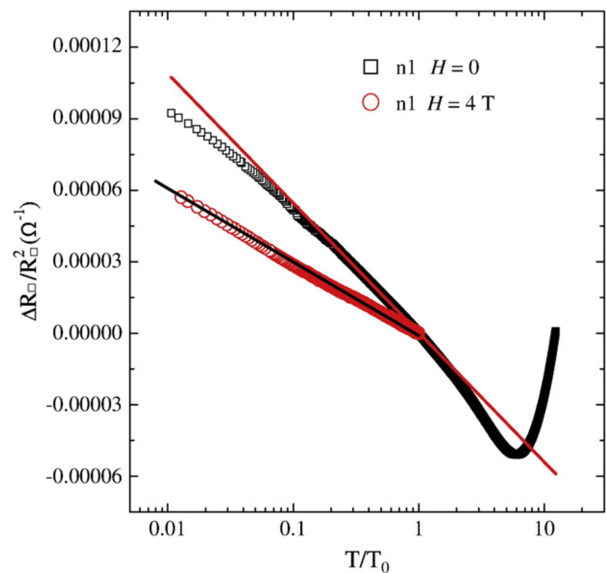

Fig. 5. Normalized sheet resistance, $\Delta R_\square(T)/R_\square^2(20\text{ K})$, as a function of normalized temperature T/T_0 ($T_0 = 20$ K) for the n1 thin film in zero magnetic field (squares) and in a perpendicular magnetic field of 4 T (circles). The straight solid lines are least-squares fits to Eq. (3).

understood in terms of a weaker temperature dependence resulting from a tendency to saturation in τ_φ [29,30]. In fact, our preliminary low-field magnetoresistance measurements indicate an exponent $p<1$ for temperatures below about 3 K. In short, the low-temperature sheet resistance rise in ITO thin films can be well explained in terms of the two-dimensional weak-localization and electron–electron interaction effects. We notice that the values of αp and $1-3F/4$ in other thin films studied in this work are similar to those in the n1 film.

4. Conclusion

We have studied the temperature dependence of resistance and thermopower in ITO thin films with various amounts of disorder. The overall temperature behavior of resistance from 300 K down to 0.3 K can be well described by the conventional Bloch–Gruneisen law, together with the contributions from the two-dimensional weak-localization and electron–electron interaction effects at low temperatures. The thermopowers are negative and linear in temperature over the whole measurement temperature range, strongly suggesting free-electron-like conduction processes in the ITO thin films. This work demonstrates that high metallic conduction can be readily achieved in RF sputtered ITO films with thickness as thin as 15 nanometers.

Acknowledgements

The authors are grateful to Shiu-Ming Huang for assistance in low-temperature measurements, and to Shih-Chun Tseng and Rong-Po Chen for performing SEM measurements. This work was supported by the Taiwan National Science Council through Grant Nos. NSC 96-2112-M-009-025 (JJL), and NSC 97-2112-M-030-001-MY2 (CYW).

References

[1] F. Matino, L. Persano, V. Arima, D. Pisignano, R.I.R. Blyth, R. Cingolani, Ross Rinaldi, Phys. Rev. B 72 (2005) 085437.
[2] C. Guillén, J. Herrero, J. Appl. Phys. 101 (2007) 073514.
[3] J. Ederth, P. Johnsson, G.A. Niklasson, A. Hoel, A. Hultaker, P. Heszler, C.G. Granqvist, A. R. van Doorn, M.J. Jongerius, D. Burgard, Phys. Rev. B 68 (2003) 155410.
[4] J. Ederth, P. Heszler, A. Hultaker, G.A. Niklasson, C.G. Granqvist, Thin Solid Films 445 (2003) 199.
[5] H. Kim, C.M. Gilmore, A. Piqué, J.S. Horwitz, H. Mattoussi, H. Murata, Z.H. Kafafi, D. B. Chrisey, J. Appl. Phys. 86 (1999) 6451.
[6] X.D. Liu, E.Y. Jiang, D.X. Zhang, J. Appl. Phys. 104 (2008) 073711.
[7] Z.Q. Li, J.J. Lin, J. Appl. Phys. 96 (2004) 5918.
[8] P. Sheng, Phys. Rev. B 21 (1980) 2180.
[9] Y.H. Lin, S.P. Chiu, J.J. Lin, Nanotechnology 19 (2008) 365201.
[10] N. Kikuchi, E. Kusano, H. Nanto, A. Kinbara, H. Hosono, Vacuum 59 (2000) 492.
[11] O.N. Mryasov, A.J. Freeman, Phys. Rev. B 64 (2001) 233111.
[12] H. Odaka, Y. Shigesato, T. Murakami, S. Iwata, Jpn. J. Appl. Phys., Part 1 40 (2001) 3231.
[13] C.Y. Wu, J.J. Lin, Phys. Rev. B 50 (1994) 385.C.Y. Wu, W.B. Jian, J.J. Lin, *ibid.* 57 (1998) 11232.
[14] D.K.C. MacDonald, Thermoelectricity: an Introduction to the Principles, John Wiley & Sons, Inc., New York, London, 1962.
[15] S. Luo, S. Kohiki, K. Okada, M. Mitome, F. Shoji, Mater. Lett. 63 (2009) 2365.
[16] A. Amaral, P. Brogueira, C. Nunes de Carvalho, G. Lavareda, Surf. Coat. Technol. 125 (2000) 151.
[17] J.M. Ziman, Electron and Phonons, Clarendon Press, Oxford, 1960, p. 364.
[18] S.P. Chiu, H.F. Chung, Y.H. Lin, J.J. Kai, F.R. Chen, J.J. Lin, Nanotechnology 20 (2009) 105203.
[19] S.S. Yeh, J.J. Lin, X.J. Jing, D.L. Zhang, Phys. Rev. B 72 (2005) 024204.
[20] K. Makise, M. Funaki, B. Shinozaki, K. Yano, Y. Shimane, K. Inoue, H. Nakamura, Thin Solid Films 516 (2008) 5805.
[21] M. Yu Reizer, A.V. Sergeev, Zh. Eksp. Teor. Fiz. 92 (1987) 2291 [Sov. Phys. JETP 65 (1987) 1291]; and private comnunications.
[22] I. Hamberg, C.G. Granqvist, K.F. Berggren, B.E. Sernelius, L. Engström, Phys. Rev. B 30 (1984) 3240.
[23] R.B.H. Tahar, T. Ban, Y. Ohya, Y. Takahashi, J. Appl. Phys. 83 (1998) 2631.
[24] H.C. Lee, Appl. Surf. Sci. 252 (2006) 3425.
[25] M.J. Alam, D.C. Cameron, Thin Solid Films 420–421 (2002) 76.
[26] A. Pokaipisit, M. Horprathum, P. Limsuwan, Jpn. J. Appl. Phys. 47 (2008) 4692.
[27] H. Morikawa, M. Fujita, Thin Solid Films 359 (2000) 61.
[28] J.J. Lin, N. Giordano, Phys. Rev. B 35 (1987) 545.
[29] J.J. Lin, J.P. Bird, J. Phys. Condens. Matter 14 (2002) R501.
[30] S.M. Huang, T.C. Lee, H. Akimoto, K. Kono, J.J. Lin, Phys. Rev. Lett. 99 (2007) 046601.
[31] P. Mohanty, E.M.Q. Jariwala, R.A. Webb, Phys. Rev. Lett. 78 (1997) 3366.